Comparative Investigations to Corrosion Fatigue of Al-Cu and Al-Mg-Si Alloys

M. Thieme[1], F. Bergner[2], I. Haase[1], H. Worch[1]

[1] Technische Universität Dresden, Institut für Werkstoffwissenschaft, D-01062 Dresden, Germany

[2] now at: Forschungszentrum Rossendorf, Institut für Sicherheitsforschung, PF 510119, D-01314 Dresden, Germany

mithi@rcs.urz.tu-dresden, F.Bergner@fz-rossendorf.de, haase-i@rcs.urz.tu-dresden.de, hworch@rcs.urz.tu-dresden.de

Introduction

One of the serious problems encountered in the use of various materials in technology is the occurrence of fatigue phenomena as an undesirable material damage under cyclic mechanical load. For aluminium alloys this issue is of extremely high importance in case of their utilisation for aircraft purposes, e.g., where a very wide spectrum of frequencies occur. Moreover, the cyclic loading may be joined by the presence of specific electrolyte media. Therefore, the material candidates must be thoroughly examined in view of their sensitivity to fatigue as well as to corrosion fatigue. Usually, the Cu-containing alloy EN-AW 2024 T3 is applied besides 7075 T6 in Airbus aircrafts, but the weldable alloy 6013 T6 is considered to be a potential alternative. Referring to former investigations on the environmental sensitivity (ES) in the fatigue behaviour /1-6/ this paper brings up experimental findings as well as expanded considerations about damaging mechanisms and modelling. The situation with the alloy 6013 T6 is emphasized. The propagation of cracks under cyclic load in different environments, such as vacuum, air or aqueous media, is described by means of fracture mechanics. This enables discrimination in view of the influence of environmental factors and, hence, the participation of corrosion processes.

Experimental

Cyclic load experiments were accomplished using a high number of aluminium alloys, partly also with different thermal treatment (Table 1). First of all, the wrought alloys EN AW-2024 T3 (cold-cured) and 6013 T6 (warm-cured) were examined. Additionally to the alloying elements as stated they may contain 0.5 wt. % Fe, about 0.5 wt. % Mn and 0.25 wt. % Zn.

EN AW- 2017 A T4	2024 T3, T81, T351, T851	2219 T87	2524 T3	5754 H22	6009 T9	6013 T4, T6	6061 T6	6082 T6	7075 T651	7475 T761	8090 T81
Al Cu4 MgSi	Al Cu4 Mg1	Al Cu6 Mn	Al Cu4 Mg	Al Mg3	Al	Al Mg1 Si0,8 CuMn	Al Mg1 SiCu	Al Si1 MgMn	Al Zn5,5 MgCu	Al Zn5,5 MgCu	Al Li2,5 Cu1,5 Mg1

Table 1: Tested Al alloys using the designations according to EN 573-1 : 1999.

The fatigue examinations were done using an Instron 8501 servo-hydraulic testing machine (conditions: sinusoidal waveform, σ_{max} =110 MPa, R = 0.1) and standard centre-cracked tension specimens (width w = 160 mm). For ES testing open Plexiglas cells (vol. 100 mL) were attached to both sides of the sheet. The electrolyte solution was 3.5 wt. % NaCl (about 0.6 mol L^{-1}). Additionally, NaCl solutions of changed pH and deionised water were used for comparison. The total frequency range was 0.004-40 Hz; survey examinations were conducted at f = 20 Hz. Crack lengths were measured using a Questar QM 100 optical microscope mounted on a computer controlled xyz stage. The tests were mostly broken off at a maximum crack length 2a of nearly 60 mm. Thus the cyclic stress intensity factor ΔK calculated according to Eq. 1 covered a range of <10 to more than 30 MPa $m^{1/2}$.

$$\Delta K = \Delta\sigma \cdot \left(\frac{\pi\, a}{\cos(\pi\, a / w)} \right)^{1/2} \qquad (1)$$

Detailed metallographic work was accomplished after finishing the loading measurements. Pieces of about 20x45 mm^2 were cut from the sheet region surrounding the crack tip (diamond abrasive saw). Qualitative and quantitative metallographic investigations were carried out using special preparing techniques, light-microscopy and SEM. Furthermore, measurements of the micro-hardness were done (load 50 mN). The concentrations of hydrogen in small volumes of the material (10x2x0.8 mm^3) were determined using hot extraction.

Results

Plotting the crack length progress per cycle da/dN vs. the cyclic stress intensity factor ΔK, the crack growth rate reveals regions of *positive* deviations in cases of environmental sensitivity (ES) in comparison to the behaviour in air, which was taken as a reference. Deionized water could be the reference as well, but no significant differences between the crack growth rates in air and deionized water were found for 6013 T6 at f = 20 Hz /2/.

In numerous fatigue experiments with aluminium alloys of different types, it has been stated that ES was low or even absent in the cases of EN AW-2024 (T3, T81, T351, T851) as well as with other Cu-alloyed aluminium materials (2017A T4, 2219 T87). Fig. 1a shows typical results for EN AW-2024 T3. Significantly increased crack growth rates in NaCl, at least over parts of the curves, were recorded for the alloys 2024 T351, 2524 T3, 5754 H22, 6009 T9, 6013 T4, T6 (Fig. 1b), 6061 T6, 6082 T6, 7075 T651, and 7475 T761. The alloys containing Li showed extraordinarily strong effects. The occurrence of ES was joined with the evolution of hydrogen bubbles in a certain phase of each loading cycle.

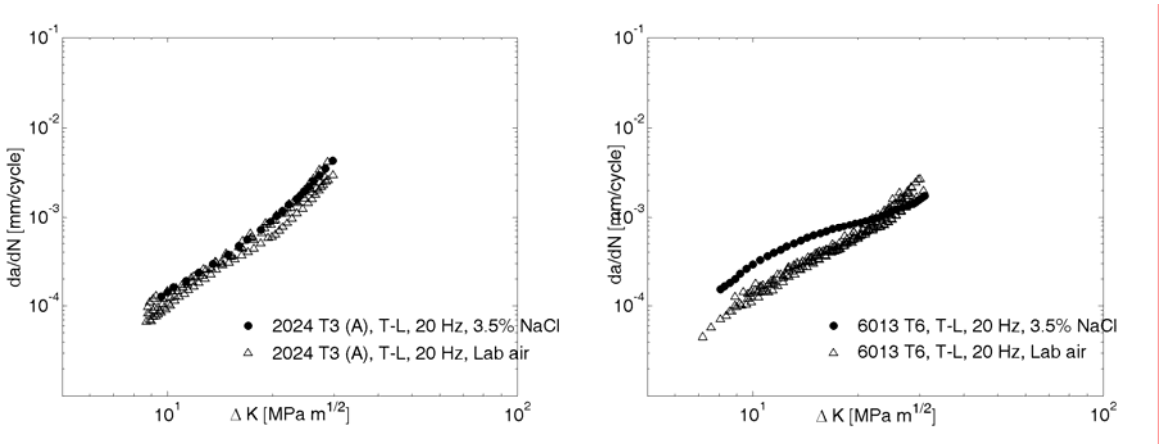

Fig. 1: Comparison of crack propagation curves for the alloys 2024 T3 and 6013 T6, each in NaCl solution (20 Hz) and at air (20 Hz), respectively.

Applying different test frequencies, ES effects are observed for 6013 T6 in a different manner. As Fig. 2a demonstrates for low f, ES becomes prominent only from medium ΔK on. At about 1 Hz increased growth rates cover the entire region. The behaviour at high f is characterized by significant effects already at the beginning of the test, whereas later on retardation is recorded so that the rates coincide to those occurring in air. These transition points of deviation or approximation were utilized for purposes of modelling (see below). It should be noticed that no ES could be measured with the extremely low frequency of 4 mHz.

The effect of ES is quantified by means of the dimensionless damage ratio $\eta = (\mathrm{d}a/\mathrm{d}N)_{\mathrm{NaCl}} / (\mathrm{d}a/\mathrm{d}N)_{\mathrm{air}}$. The plot of η vs. f (Fig. 2b) summarizes the statements given in view of the frequency dependencies.

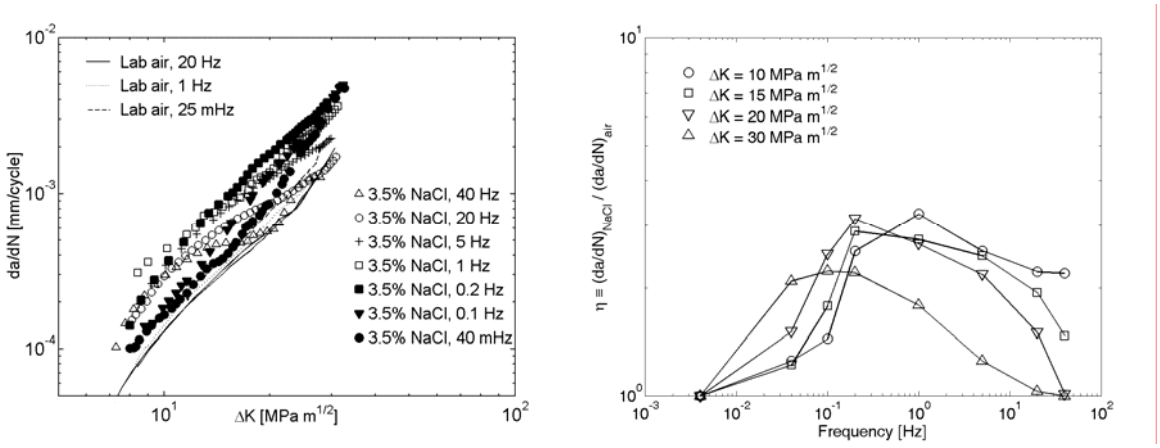

Fig. 2: *a*) Crack propagation curves for the alloy 6013 T6 recorded under varied test frequency in NaCl solution and at air, respectively (*left*); *b*) Plot of the damage ratio η vs. frequency for different values of the cyclic stress intensity factor ΔK (*right*).

Moreover, experiments with 6013 T6 and a NaCl-HCl solution of pH = 1 showed increased crack propagation even at high ΔK values. On the other hand, pH = 11 gave a behaviour similar to that with air.

Different metallographic methods were utilized to clear up consequences of the cyclic loading and to elucidate possible reasons for ES originating from micro-structural features. Microscopic observations showed that the alloy 6013 T6 contained relatively coarse intermetallic phases (Fig. 3) /3, 4/. Their composition and structure corresponded to the type $Al_{19}Fe_4MnSi_2$. The cyclic loading in NaCl medium led to decohesion effects and fractures in these particles themselves as well as to initiation of cracks starting from these points. The number of the fractured precipitations was found to be dependent on the test frequency, with a significant maximum at some medium frequency (ca. 5 Hz). It could be indicated that these precipitations interacted with surrounding matrix under generation of a local

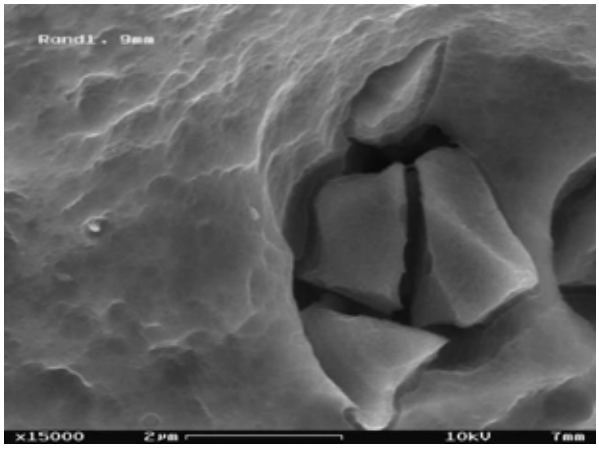

Fig. 3: SEM images of coarse precipitations located in the flank of a crack; 6013 T6, NaCl medium, $f = 1$ Hz, $\Delta K \approx 30$ MPa m$^{1/2}$.

element with the iron-rich particle forming the cathode. Furthermore, hydrogen analysis suggested that the interface between these particles and the matrix causes trapping effects.

Moreover, the studies showed increased values of the micro-hardness determined in regions around the crack tip, but even very near to the crack edges. These findings agree with those from hydrogen analysis. Finally, tendencies to the formation of secondary cracks were observed /3, 4/. All these phenomena were characterized by a marked dependence on the frequency with more or less pronounced maxima occurring at medium *f* (about 1 Hz).

Discussion

Mechanistic considerations

Considering the different crack propagation types of the aluminium alloys examined, it is supposed that the composition of the alloys act via their microstructural states, which are influenced by the nature and the global content of the alloying elements as well as by thermal processing. This approach is supported by the fact that the solubility of the most alloying components in Al is very limited only (depending on *T*), with the exception of binary Al-Mg alloys of up to about 5 wt. % Mg /7/. Therefore, the formation of precipitations is favoured in practically every case. Nature, origin and size of the precipitations are varying in a very broad range. However, it is well-known that the equilibrium phases, such as Al_2Cu or $MgSi_2$, are *generally not present* in cured Al alloys. The strong increase of strength and hardness is rather caused by nanoscalic phases of different degrees of coherence, among them the so-called Guinier-Preston zones. Their composition may not be simply expressed as a formula. Clearly, this situation must be taken into account when the experimental results with different materials are discussed from the view of corrosion science. The participation of precipitations in electrochemically based damage mechanisms is considered under focus onto the well-defined intermetallics /8/. Buchheit /9/ compiled potential data for a range of intermetallics and binary alloys.

At first a more principal consideration to potential electrochemical processes involved in the damage will be outlined. Later on the mechanistic discussion will be expanded implementing effects of the cyclic mechanical loading.

In the course of crack growth, a bare metal surface is formed. Fresh Al will undergo *anodic reactions* where different paths should be possible. The usual anodic dissolution (AR1) produces highly charged ions (Eq. 2a) so that a stepwise hydrolysis joined by acidification will follow (Eq. 2b).

$$\text{AR1:} \qquad Al \rightarrow Al^{3+} + 3e^-; \qquad Al^{3+} + x\ H_2O \leftrightarrow Al(OH)_x^{3-x} + x\ H^+ \qquad (2a,b)$$

Furthermore, the anodic partial reaction may also directly conduct to the growth of an oxidic film ('Al_2O_3', Eq. 3). This is more probable under less acid conditions.

$$\text{AR2:} \qquad 2\ Al + 3\ H_2O \rightarrow Al_2O_3 + 6\ H^+ + 6\ e^- \qquad (3)$$

Generally, passivating reactions proceed with a high rate according to experience with simultaneous grinding or scratching of the surface. Because of the self-inhibiting properties of this film, the rate will quickly decrease. As a competing reaction in the presence of strongly chemisorbing and complexing anions, such as Cl^-, the following reaction must be additionally taken into account:

$$\text{AR3:} \qquad Al + n\ Cl^- \rightarrow AlCl_n^{3-n} + 3\ e^- \qquad (4)$$

The corresponding *cathodic partial reactions* may be imagined via different routes, likewise. Reductive reactions under release of elemental hydrogen are expected to play a *key role* in view of the finding that increased hydrogen concentrations were found in material regions near the crack. However, released hydrogen enters the metal lattice in *statu nascendi* only, i.e. in the *monoatomic* state. Hydrogen leads to serious embrittlement and, hence, promotes crack growth and, finally, fracturing. It should be noticed that the transfer of H into the metal will be strongly hampered by even very thin oxide films, as was experimentally stated for a number of metals /10/. Therefore, this transfer will occur essentially at bare metal surfaces. Lattice transport is based on diffusion and dislocation movement. Clearly, diffusion will be supported in the case of strained microstructural sites in the forefront of the crack tip.

The usual discharge of H_3O^+ ions (CR1) is promoted in case of an acidified medium. In addition, the O_2 reduction (CR2) can take part under aerated conditions. Cathodic reactions can principally proceed also on sites which are covered with a thin oxidic film (Al as a valve metal), such as the flanks of the crack or the outer surface of the sheet specimen. However, the greater the distance to the local anode, the thicker the film and the lower the conductivity of the electrolyte solution, the less will be the contribution of these sites to the net flow of charge. Therefore, it is assumed that the effective cathodic area will be limited to the neighbourhood of the crack tip, with a relation of the areas of $A(\mathrm{CR}) > A(\mathrm{AR})$. By the way, both CR1 and CR2 lead to partial alkalization. This is turn can be cause an attack of Al (Eq. 5a) due to its amphoteric properties, but also on oxidized areas (Eq. 5b).

$$\mathrm{Al} + y\ \mathrm{OH^-} + 3\ \mathrm{H_2O} \rightarrow \mathrm{Al(OH)_{3+y}^{y-}} + 3/2\ \mathrm{H_2} \qquad (5a)$$

$$\mathrm{Al_2O_3} + 2y\ \mathrm{OH^-} + 3\ \mathrm{H_2O} \leftrightarrow 2\ \mathrm{Al(OH)_{3+y}^{y-}} \qquad (5b)$$

These reactions are conceivable to proceed with Al materials generally, even with Cu-alloyed ones without ES as well as with other materials showing ES. Discrepancies in corrosion fatigue must be ascribed, therefore, to *effects of precipitations* including G-P zones as specific features of the different materials. It is well-known from electrochemical kinetics that the exchange current density for the H_3O^+ reduction (CR1) as well as the rate of the recombination of the primarily discharged H atoms to H_2 are strongly substrate-dependent /11,12/. Thus, the intensity of the hydrogen generation depends not only on the area of the cathodic sites. It is felt that there are significant influences from the nature of the metal, where the cathodic reaction is proceeding. Moreover, it may be concluded that the entrance of *monoatomic hydrogen* into the solid is supported or not by its electrokatalytic properties.

In the case of the alloy 6013 T6, *coarse intermetallic phases* of the type $Al_{19}Fe_4MnSi_2$ has been found /3,4/. They are characterized by a size in the lower µm region (Fig. 3) and form the cathode (CR1,2) in a local element with the surrounding Al matrix. Hydrogen was found to be trapped there. Maybe, the latter also contributes to embrittlement.

On the other hand, the range of *nanoscalic, finest dispersed precipitations* as a result of the curing treatment get contact to the electrolyte solution, at least near the progressing crack tip. As for magnesium-containing precipitations, such as metastable 'Mg_2Si', it is hardly conceivable that they will take part in a CR because of their negative potential /9/. However, variants of pathways were examined from a thermodynamic point of view. Magnesium hydride was assumed as an intermediary product, which easily decomposes in aqueous solutions releasing hydrogen /13/. The simultaneous formation of elemental silicon is supported by experimental findings from model experiments using compact Mg_2Si. The hypothetical gross reaction acc. to Eq. 4a, which is the result of a superposition of cathodic

and anodic reactions of the corresponding local element, should indeed be possible in view of its negative Gibbs reaction energy ΔG_{r6a}^{o} (298 K).

$$3\ Mg_2Si + 4\ Al + 6\ H_2O \rightarrow 6\ MgH_2 + 3\ Si + 2\ Al_2O_3 \qquad -1737\ kJ \qquad (6a)$$

However, the comproportionation of hydride and H^+ under formation of *monoatomic* hydrogen is characterised by a *positive* figure for ΔG_{r6b}^{o}, which has an overcompensating effect:

$$6\ MgH_2 + 12\ H_2O \rightarrow 6\ Mg(OH)_2 + 24\ H \qquad +2941\ kJ \qquad (6b)$$

A similar result is obtained for another, simple redox scheme, where Si^{-4} from the silicide is assumed to reduce H_2O to atomic hydrogen. The total sum would be positive again: $\Delta G_r^{o} = 169\ kJ\ mol^{-1}$. On the contrary, a completely changed situation is obtained in view of the energetic balance when H_2 molecules form the product, as for the example of Eq. 7:

$$Mg_2Si + 4\ H_2O \rightarrow 2\ Mg(OH)_2 + Si + 2\ H_2 \qquad -644\ kJ \qquad (7)$$

That means, a reaction under formation of hydrogen exclusively as monoatomic species appears to be not possible from thermodynamics. Rather, part of the evolved hydrogen must be diatomic. As mentioned, the latter will not contribute to embrittlement. The suggested sequence may be characteristic for precipitations containing Mg and Si, but not for the precipitations and GP zones typical for Cu-alloyed Al materials.

Taking into account that these corrosion processes proceed in the course of cyclic mechanical loading, it is obvious that there may be influences from this side. In the first phase of *increasing tension* ($t_0 = t_{min}$ to $t_1 = t_{max}$) the actual stress intensity factor at the existing crack tip will also increase resulting in the continuation of growth beyond a critical value, thus producing a bare metallic surface. Here the reactions mentioned above will proceed. A tentative assessment of the relative rates of the single steps lead to the conclusion that the *oxide formation* and/or the *phase transition of atomic H* may be the *rate controlling step* (RCS), while the subsequential lattice diffusion will be faster, especially under the conditions of lattice dilatation under the increased tension.

In the second phase of *decreasing tension* (t_1 to $t_2 = t_0$) the crack growth is supposed to go down. Likewise, the rate of the anodic reactions will diminish, as the film thickness increases. Depending on the complexing power of Cl^- and pH the dissolution of the oxide will act

$$Al_2O_3 + 2n\ Cl^- + 6\ H^+ \leftrightarrow 2\ AlCl_n^{3-n} + 3\ H_2O \qquad (8)$$

The solid state diffusion of H can still proceed, but will slow down, as the transfer rate of hydrogen acc. to CR1 and the hypothetical Eq. 6b diminish.

Of course, if the supposed coordination of mechanical and corrosive actions was true, an influence of time and, hence, of frequency must be discussed additionally. The numerous dependencies of the frequency of the loading tests, as stated above, suggest such an assumption. Obviously, at low *f* and low progress of crack growth during the interval (t_1 - t_0) the diffusion rate of hydrogen in the solid may be high enough to escape. Critical concentrations and embrittlement effects at the crack tip leading to enhanced propagation rates arise only *beyond* the starting phase (Fig. 2a). Contrarily, at medium *f* the time interval decreases and the distance covered by the diffusing H atoms within this period is smaller. This will cause a concentrating effect of the hydrogen atoms, similar to a tailback. At high *f*, finally, the critical H concentration is reached at the very beginning of the crack growth process. This is seen as a result of the increasing part of strengthening effects, which will facilitate the entrance of H atoms into the metal. However, the time interval has further shor-

tened so that the amount of H per cycle will *decrease* /3/ counteracting the favouring tendencies. This matter of fact is regarded as one of the decisive reasons that *maxima* are formed in the frequency dependencies of the damage ratio η (Fig. 2b). As mentioned above, this is reflected also in the frequency-dependent behaviour of other parameters, such as the hydrogen concentration in the crack tip neighbourhood, the micro-hardness, and the formation of secondary cracks /3,4/. In each case maxima were found at some medium frequency.

Quantitative Modelling

Quantitative modelling was accomplished on the basis of the experimental findings of crack propagation in the presence of NaCl solutions vs. air. Methodically, it makes use of dimensional analysis. The model is based on the assumption of a multiple-step mechanism being responsible for the increased crack growth rates and the *concept of a rate-controlling step* (RCS) /14/. Three potential RCS have been taken into account. Each one of them is considered to be characterized by a single (or effective) physical quantity. Their dimensions are: $1/T$, L/T, and L^2/T, where T and L denote time and length, respectively. In the context of the above considerations, these quantities can be interpreted as follows: i) the *rate of production q* of a *damaging species*, which may act directly (in the case of hydrogen) or indirectly (chloride ions) by destabilizing a protecting surface layer, ii) the *rate of thickness growth v* of a surface layer on the freshly formed metal surface and iii) an *effective coefficient of diffusion D* of hydrogen to the embrittlement sites in front of the crack tip or to transporting dislocations. However, it is important to notice that the formalism depends only on the physical dimensions of these quantities, but not on the nature of the presumably underlying processes themselves. The formalism consists of the following steps [5]: i) According to the experimental observations and the above assumptions, the damage ratio η was considered as a function of ΔK, E, f, and either q, or v, or D. ii) The dimensional analysis was applied to these three cases. *Linear* relations between η and q, v^{-1} and the mean diffusional path, $(D/f)^{1/2}$, respectively, were assumed (C_a, C_b, and C_c dimensionless constants):

$$\eta_a = C_a\left(f^{-1}\ q\right), \quad \eta_b = C_b\left(\Delta K^2\ E^{-2}\ f\ v^{-1}\right), \quad \eta_c = C_c\left(\Delta K^{-2}\ E^2\ f^{-1/2}\ D^{1/2}\right) \quad (7a,b,c)$$

iii) In order to identify the ranges of ΔK and f, where a certain step is the slowest one, the above expressions were equated to one another. In a double-logarithmic f-ΔK plot the resulting power-law equations between ΔK and f are represented by straight lines, which separate the regions in the plot, where the respective steps are rate controlling. iv) The lines defined by the conditions $\eta = 1$ bound these regions against the surroundings, where no environmental effect is present. v) To obtain a graphical representation of the 'rate-control map', frequency f and stress intensity factor range ΔK had to be normalized by the model parameters f_S and ΔK_S. The resulting rate-control map is presented in Fig. 4a. This representation may be imagined as the ground-plan (projection on the plane η =1) of a three-dimensional plot f_S - ΔK_S - η with intersecting planes. A three-sided pyramid is thus formed from those partial areas corresponding to the *lowest* η for a given f_S - ΔK_S pair. This *process-competition* is equivalent to the mathematical expression $\eta = \max[1,\min(\eta_a, \eta_b, \eta_c)]$.

The individual mechanistic steps which underlie these constructions will control the overall rate of crack propagation in the respective regions. That means, an experiment with a fairly high f would be controlled at first by any retarding action (e.g. of film growth), afterwards by the intensity of the source (the entrance of H atoms into the metal lattice) and finally by the diffusion process (of H atoms).

An additional step was accomplished towards an advanced description of reality by replacing pure process-competition by a kind of *superposition* /15/. Applied to the present situation

Eq. (9) was obtained /6/, where the fractional term on the right-hand side can be imagined as analogue of the conductivities in a series of electric resistors. In this way, the edges and the tip of the mentioned pyramid are transformed to 'soft' transitions due to the simultaneous dominance of two or three steps. The result is shown in Fig. 4b for the Al alloy 6013 T6.

$$\eta = 1 + \frac{1}{1/\eta_a + 1/\eta_b + 1/\eta_c} \tag{9}$$

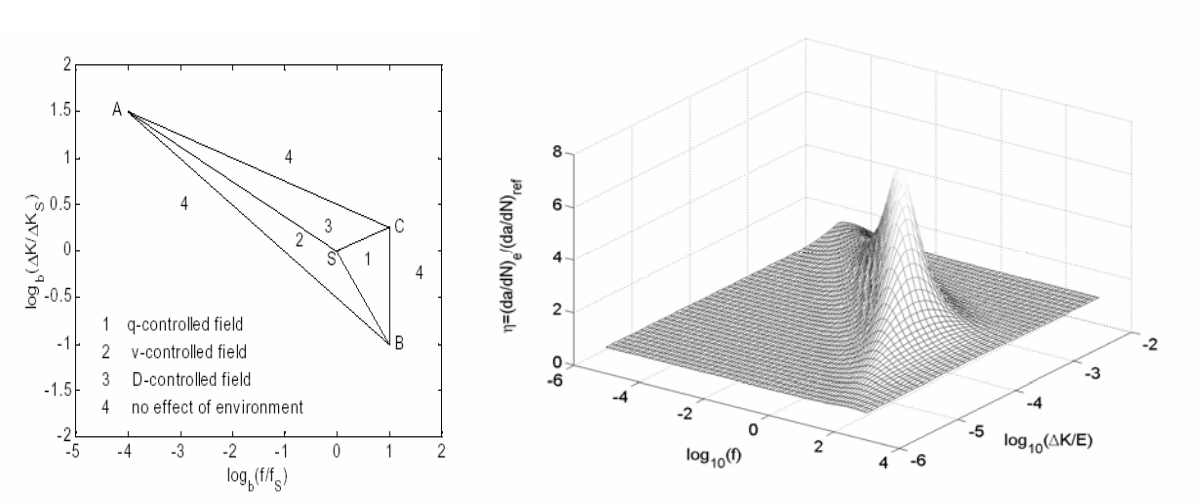

Fig. 4: Rate-control maps as results of the present formalism. *a*) Normalized double-logarithmic plot /5/; *b*) 3D 'softened' plot applied for the Al alloy 6013 T6 /6/.

The formalism applied in the present paper is generally applicable to any number of rate-controlling steps and it works for any combination of independent physical dimensions. Of course, the present model of environment-sensitive fatigue crack growth is influenced by the nature of the rate-controlling steps through the dimensions of the characteristic quantities.
The conclusions derived from modelling confirm and expand the more intuitive assumptions from an electrochemical point of view, which of the steps may be rate-controlling. The chosen approach allows to calculate those physical quantities characterizing the individual RCS. Finally, it gives precise predictions, whether or not ES will be present depending on f and ΔK.

References

/1/ I. Trockels, G. Lütjering, A. Gysler, Mat. Sci. Forum 217-222 (1996) 1599.
/2/ K. Nocke, F. Bergner, H. Bersch, I. Haase, H. Worch, G. Tempus, E. Loechelt, Mater. Corros. 51 (2000) 628-634.
/3/ I. Haase, K. Nocke, H. Worch, G. Zouhar, G. Tempus, Prakt. Metallogr. 38 (2001)119-137.
/4/ I. Haase, K. Nocke, M. Ruhnow, H. Worch, ibid. 38 (2001) 647-660.
/5/ F. Bergner, H. Bersch, H. Worch, G. Zouhar, Intern. J. Fatigue 24 (2002) 831-839.
/6/ F. Bergner, Proc. 14th European Conf. of Fracture, Kraków, 2002.
/7/ E. Hornbogen, Werkstoffe, Berlin: Springer 1991, pp. 238-243.
/8/ O. Seri, in: M. Schütze (ed.), Corrosion and Environmental Degradation, Vol. II, Weinheim: Wiley-VCH, 2000, pp. 117-129.
/9/ R. G. Buchheit, J. Electrochem. Soc. 142 (1995) 3994-3996.
/10/ K.-H. Müller, unpubl. lecture, Dresden, Oct. 2001.
/11/ K.-H. Tostmann, Korrosion, Wiley-VCH, 2001, pp. 68-69.
/12/ W. Forker, Elektrochemische Kinetik, Berlin: Akademie-Verlag, 1966, pp. 129-137.
/13/ H. Remy, Lehrbuch der anorganischen Chemie, Bd. 1, Leipzig: Geest&Portig, 1965, p. 584.
/14/ R. P. Gangloff, R. P. Wei, Metall. Trans. A 18A (1977) 1043-1053.
/15/ R. P. Wei, J. D. Landes, Mater. Res. Stand. 9 (1969) 25-28.